

The effect of submarine melting on calving from marine terminating glaciers

Yue Ma¹, and Jeremy N. Bassis²

¹Physics Department, University of Michigan, Ann Arbor, Michigan, USA.

²Climate and Space Sciences and Engineering, University of Michigan, Ann Arbor, Michigan, USA.

Key Points:

- We simulate the interplay between submarine melt and calving using a 2D model of a marine terminating glacier.
- Submarine melt can enhance or suppress calving, but the total mass lost (usually) increases.
- The magnitude and vertical distribution of submarine melt profile determine if melt enhances or suppresses calving.

This is the author manuscript accepted for publication and has undergone full peer review but has not been through the copyediting, typesetting, pagination and proofreading process, which may lead to differences between this version and the [Version of Record](#). Please cite this article as doi: [10.1029/2018JF004820](https://doi.org/10.1029/2018JF004820)

Corresponding author: Yue Ma, yuema@umich.edu

Abstract

Submarine melting and iceberg calving are two important processes that control mass loss from the terminus of tidewater glaciers. There have been significant efforts to quantify the effect of submarine melting on glacier calving, but controversy remains with conflicting studies indicating submarine melting can increase, decrease, or has minimal effect on calving. Here we show using a two-dimensional full Stokes finite element model that submarine melt can alter the state of stress near the terminus and the changes in stress exert a first-order control on the calving regime of marine terminating glaciers. The model calculates both the largest principal and maximum shear stresses and then maps out where tensile and shear failure occur for a range of melt rates and vertical melt profiles. We find that submarine melt initially promotes full-thickness calving events. However, as the melt rate further increases, an overhang begins to form and resulting compressive stresses suppress full thickness calving. These results are relatively insensitive to basal friction. Moreover, our results suggest that submarine melting can both increase and decrease calving rates with the magnitude and sign of the effect determined by the shape of the melt profile and the relative magnitude of average melt rate. Despite the fact that calving is suppressed in some circumstances, the addition of submarine melt almost always increases the total mass loss. Overall, we find that relatively small amounts of submarine melt can destabilize glaciers, but calving and frontal ablation are increasingly controlled by submarine melt as it continues to increase.

1 Introduction

Iceberg calving and submarine melting are two important processes that occur at the interface between a marine terminating glacier and the ocean. Together, calving and submarine melting—collectively called ‘frontal ablation’—account for nearly half of the total mass lost from the Greenland Ice Sheet [Rignot *et al.*, 2008; van den Broeke *et al.*, 2009; Enderlin *et al.*, 2014]. Despite this important role, our understanding of both processes and, in particular, the interaction between submarine melting and iceberg calving remains limited with different studies finding contradictory relationships [Motyka *et al.*, 2003; Röhl, 2006; Rignot *et al.*, 2010; Bartholomaus *et al.*, 2013; O’Leary and Christoffersen, 2013; Cook *et al.*, 2014; Todd and Christoffersen, 2014; Krug *et al.*, 2015; Luckman *et al.*, 2015; Rignot *et al.*, 2016; Truffer and Motyka, 2016]. For example, O’Leary and Christoffersen [2013] took a diagnostic approach to examine how frontal melting promotes calving. By

45 developing a two-dimensional finite element model, they concluded that the shift in stress
46 contours resulting from fixed undercutting with various shapes at the terminus is likely
47 to increase calving and is insensitive to the choice of calving law, basal condition (un-
48 less floating) or ice thickness. However, their model was limited by its purely diagnostic
49 nature; stress was computed based on rectangular glaciers with specified calving front pro-
50 files without accounting for the co-evolution of the calving front morphology with melt
51 and ice dynamics. In contrast, several studies allowed calving front morphology to evolve
52 in response to an applied melt rate [Cook *et al.*, 2014; Todd and Christoffersen, 2014; Krug
53 *et al.*, 2015]. These studies used more realistic geometries and forcing to examine the role
54 of submarine melting in determining glacier terminus positions. For instance, Cook *et al.*
55 [2014] modeled Helheim Glacier and found that in their simulations, terminus behavior is
56 not sensitive to the presence of submarine melt unless unrealistically large melt rates were
57 prescribed. Similarly, Todd and Christoffersen [2014] focused on Store Glacier and arrived
58 at a conclusion that submarine melting has a limited effect on calving behavior. In this
59 case, the terminus was perched atop a thick sill and located near a bottleneck in the fjord.
60 Todd and Christoffersen [2014] also reported that despite a slight increase in calving fre-
61 quency with submarine frontal melting, the simulated size of calving events decreased as
62 submarine melting increased. However, in a more recent study of the same glacier, Todd
63 *et al.* [2018] concluded using a 3D model that concentrated plume melting has a desta-
64 bilizing effect on the calving front position. In contrast, Krug *et al.* [2015] examined a
65 variety of glacier geometries as well as melt rates and argued that frontal melting did im-
66 pact terminus behavior on a seasonal time scale, but had no effect on inter-annual mass
67 loss. They too concluded that undercutting grounded glaciers increased calving frequency,
68 but reduced calving size. More recently, Benn *et al.* [2017] examined the relationship be-
69 tween calving and submarine melting at the calving front using discrete element models
70 that simulate both flow and fracture combined with finite element models of the viscous
71 flow. They found that submarine melt could significantly alter the size of calving events
72 and this effect became dramatically larger as glaciers (or parts of glaciers) became hydro-
73 statically unstable (super-buoyant).

74 Observational studies have been equally conflicted. For instance, Luckman *et al.*
75 [2015] discovered a linear dependency of frontal ablation (the combination of subma-
76 rine melt and calving) on ocean temperature among three Svalbard tidewater glaciers.
77 Bartholomaeus *et al.* [2013] found that the large submarine melt rates during the summer

78 of Yaktse Glacier, Alaska accounted for nearly all of the mass loss from the terminus
79 region with only a small contribution from calving. This suggests that, at least for these
80 glaciers, submarine melting is the dominant process controlling frontal ablation. However,
81 observations also show that frontal ablation strongly correlates with near terminus velocity
82 [van der Veen, 2002]. In this case, it is unclear why submarine melt, largely controlled by
83 ocean properties, would correlate with terminus velocity, which is determined by ice dy-
84 namics. Furthermore, melt rates in many cases are much smaller than daily ice flow veloc-
85 ities, which can be up to tens of meters per day at many rapidly flowing outlet and tide-
86 water glaciers [Rignot and Kanagaratnam, 2006; Moon *et al.*, 2012, 2014]. For example,
87 terminus velocities for Jakobshavn Isbræ approach 34 m/day [Joughin *et al.*, 2004, 2008]
88 whilst submarine melt rates are no greater than 3 m/day [Enderlin and Howat, 2013]. This
89 has led researchers to suggest that submarine melt is less important—or negligible—for
90 these large outlet glaciers.

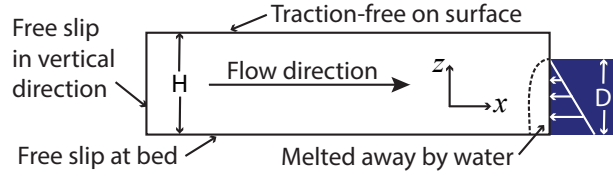
91 Here we seek to address this controversy using an idealized glacier model to simu-
92 late the interaction between submarine melting, ice dynamics, and calving. Our model, a
93 two-dimensional Stokes flow based on the finite element analysis (described in more detail
94 below), was developed to examine both tensile and shear failure regimes within glaciers
95 and tracks the growth of surface and basal crevasses [Ma *et al.*, 2017]. In this study we
96 apply a similar methodology, but additionally prescribe submarine melting to examine
97 how erosion of the calving front alters the shape of the glacier and through it, the stress
98 regime.

99 **2 Model description**

100 For computational simplicity and to illuminate relevant processes, we focus on a
101 two-dimensional flow model that consists of a vertical cross-section which cuts along the
102 central flow line of a glacier (Fig. 1). We use this two-dimensional model to characterize
103 calving behavior, focusing on the near terminus region where icebergs detach.

109 **2.1 Ice dynamics**

110 As described in Ma *et al.* [2017], the full Stokes system we are solving can be repre-
111 sented as the conservation of linear momentum in both x and z directions and the incom-



104 **Figure 1.** A schematic of the two-dimensional model domain with boundary conditions labeled. The white
 105 rectangle represents ice (thickness $H = 800$ m) and the blue rectangle ocean (depth $D = 700$ m). The flow
 106 of ice is from left to right in the figure. Our idealized domain consists of (initially) rectangular glaciers on
 107 flat beds. Our model neglects basal topography and lateral drag to better isolate the near terminus processes
 108 associated with submarine melt.

112 pressibility of glacier ice:

$$\frac{\partial \tau_{xx}}{\partial x} + \frac{\partial \tau_{xz}}{\partial z} = \frac{\partial p}{\partial x}, \quad (1)$$

$$\frac{\partial \tau_{xz}}{\partial x} + \frac{\partial \tau_{zz}}{\partial z} = \frac{\partial p}{\partial z} + \rho_i g, \quad (2)$$

$$\frac{\partial u}{\partial x} + \frac{\partial w}{\partial z} = 0. \quad (3)$$

113 Here we denote the components of the deviatoric stress tensor by τ_{ij} where $(i, j) = (x, z)$,
 114 pressure by p , density of ice by ρ_i (see Table 1), and gravitational acceleration by g , with
 115 x representing the along-flow coordinate and z representing the vertical coordinate, as il-
 116 lustrated in Fig. 1.

117 The connection between strain rate and deviatoric stress is given by the rheology of
 118 ice, in the form of a power-law [Glen, 1955; Nye, 1955],

$$\tau_{ij} = B \dot{\epsilon}_e^{\frac{1-n}{n}} \dot{\epsilon}_{ij} \quad (4)$$

119 where $\dot{\epsilon}_{ij}$ denotes the strain rate components and $\dot{\epsilon}_e$ denotes the second strain rate invari-
 120 ant, defined by $2\dot{\epsilon}_e^2 = \dot{\epsilon}_{ij}\dot{\epsilon}_{ij}$. Here B is the temperature-dependent creep parameter defined
 121 in *van der Veen* [2013] Chapter 2 (see Table 1) and $n = 3$ denotes the creep exponent.

122 There are four boundary conditions that need to be defined: surface, bed, upstream, and
 123 downstream/terminus. Because atmospheric pressure is (nearly) constant over the glacier,
 124 the ice-air interface is treated as traction free. Moreover, since we only consider short time
 125 intervals such as months to a year, we do not include surface mass balance in our simula-
 126 tions. At the ice-water interface (terminus), we insist on continuity of traction, assuming
 127 that ocean water is in hydrostatic equilibrium. Because our primary interest is in grounded
 128 tidewater glaciers, we focus only on the evolution of glaciers up to flotation. Once the ice

129 thickness reaches buoyancy, the model is stopped. At the bed, we apply a Newtonian slid-
130 ing law with a constant friction coefficient μ :

$$f = \mu u. \quad (5)$$

131 We considers two cases. The first case corresponds to negligible resistance from sliding
132 ($\mu = 0$), while the second case incorporates sliding appropriate for a fast flowing outlet
133 glaciers (see Table 1).

134 For the upstream (inflow) boundary condition, we assume free-slip in the vertical
135 direction and zero horizontal inflow velocity. Both tensile and shear stress fields are cal-
136 culated diagnostically and examined to determine where failure occurs. The failure crite-
137 ria we apply are described below in Section 2.2 and the model numerics are described in
138 more details in Section 2.4.

139 2.2 Failure criteria

140 In the section above we have focused on the deviatoric stress. However, the failure
141 criteria are based on the Cauchy stress and we examine both tensile and shear stresses
142 [Ma *et al.*, 2017]. The relationship between Cauchy stress σ and deviatoric stress τ is sim-
143 ple:

$$\sigma_{ij} = \tau_{ij} - p\delta_{ij} \quad (6)$$

144 where p is the pressure and δ_{ij} is the Kronecker delta. The eigenvalues of the Cauchy
145 stress tensor give the two principal stresses

$$\sigma_{\max, \min} = \frac{\sigma_{xx} + \sigma_{zz}}{2} \pm \sqrt{\left(\frac{\sigma_{xx} - \sigma_{zz}}{2}\right)^2 + \sigma_{xz}^2} \quad (7)$$

146 The difference between the two principal stresses gives the maximum shear stress

$$\tau_{\max} = \frac{1}{2}(\sigma_{\max} - \sigma_{\min}) = \sqrt{\left(\frac{\sigma_{xx} - \sigma_{zz}}{2}\right)^2 + \sigma_{xz}^2} \quad (8)$$

147 Because crevasses are largely tensile fractures, high tensile stress naturally promotes
148 their growth. Following previous work [e.g., Nye, 1955; Benn *et al.*, 2007; Nick *et al.*,
149 2010], crevasses grow when the largest principal stress σ_{\max} is positive and penetrate to
150 the depth where the largest principal stress becomes compressive. This model, frequently
151 termed the ‘Nye zero stress’ model, corresponds to the assumption that (i) crevasses are
152 closely spaced so that they do not significantly alter the large-scale stress field and; (ii)
153 pre-existing flaws are prevalent allowing crevasses to initiate anywhere and penetrate to

154 the deepest portion of the glacier permissible based on the stress regime. We include both
155 surface and basal crevasses in our treatment. Surface crevasses in our model are assumed
156 to be water-free. The presence of water in surface crevasses would enable them to pen-
157 etrate more deeply, but few measurements exist that constrain water depth in crevasses.
158 Moreover, iceberg calving events do occur in regions and time periods where atmospheric
159 temperatures are too cold to support water filled crevasses. Basal crevasses near the ter-
160 minus are assumed to be connected to the ocean and thus filled by seawater. Hence, wa-
161 ter pressure from the ocean is added to the existing stress field for the area of the glacier
162 below the waterline, analogous to the treatment by *Benn et al.* [2017]. Therefore, zones
163 where the largest principal stress is positive ($\sigma_{\max} > 0$) suggest areas where crevasses
164 can exist, with the zero stress contour marking the boundary between crevassed and un-
165 crevassed ice.

166 High shear stress also promotes failure along faults. Ice has been postulated to fail
167 when the maximum shear stress τ_{\max} exceeds the shear strength, which field and labo-
168 ratory studies suggest falls in the range of 500 kPa to 1 MPa [*Frederking et al.*, 1988;
169 *Schulson*, 1999; *Petrovic*, 2003; *Bassis and Walker*, 2012; *Morlighem et al.*, 2016]. We use
170 a value of 500 kPa in our model. Similar to how we treat tensile stress, again assuming
171 dense pre-existing flaws and narrow faults, the maximum shear stress is calculated and ar-
172 eas of high shear stress, i.e. with values above the shear strength of ice ($\tau_{\max} > 500$ kPa),
173 are identified.

174 In addition to the above two stress criterion, we assume that the history of the ice
175 can affect its current state. Studies have shown that crevasses generally remain open dur-
176 ing glacier advection for about 1-2 years [*Harper et al.*, 1998; *Colgan et al.*, 2016], which
177 is longer than or at least equivalent to the time scale we consider in this study (several
178 months to a year). Therefore, once ice becomes crevassed in the model, we assume it
179 stays crevassed. The area of crevassed (failed) ice at any time step is the sum of that from
180 all the previous time steps, reflecting the history of the glacier stress field.

181 **2.3 Imposed submarine melt**

182 High-resolution three-dimensional ocean circulation models can describe submarine
183 melting, but the demand for high computational power as well as the uncertainty in ap-
184 propriate far field forcing and local subglacial discharge associated with these simulations

185 makes simplified profiles more suitable for our purpose. Here we approximate submarine
 186 melting using three idealized melt profiles and compare glacier response to different pro-
 187 file shapes and average melt rates.

188 Some studies have shown melt rates reaching a maximum near the lower part of
 189 the calving front caused by the penetration of warm, dense intermediate waters that are
 190 quickly cooled by the entrainment of cold, fresh water generated by ice melt [e.g., *Xu*
 191 *et al.*, 2013; *Sciascia et al.*, 2013; *Rignot et al.*, 2015]. To approximate this type of profile
 192 we assume the submarine melt rate increases linearly from 0 at the waterline to a maxi-
 193 mum value at the bed:

$$\dot{m} = 2\bar{m}\left(1 - \frac{z}{D}\right) \quad (9)$$

194 where \bar{m} is the depth-averaged value of the melt rate, D is the water depth, and z is the
 195 vertical position with $z = 0$ at the bed and $z = D$ at the waterline.

196 In contrast, a melt rate maximum near the middle part of the calving front is also
 197 possible [e.g., *Sciascia et al.*, 2013; *Rignot et al.*, 2015; *Slater et al.*, 2017], with shapes of
 198 melt profiles resembling a parabola. In this case, the melt rate is zero both at the waterline
 199 and the bed and reaches a maximum between the bed and ocean surface. We approximate
 200 this melt profile as follows:

$$\dot{m} = 6\bar{m}\frac{z}{D}\left(1 - \frac{z}{D}\right). \quad (10)$$

201 Finally, the third choice is simply a uniform melt profile where the melt rate stays
 202 constant from the waterline to the bed:

$$\dot{m} = \bar{m}. \quad (11)$$

203 Constant melt may be representative of shallow termini or really warm waters found in
 204 some Alaskan fjords.

205 These melt profiles are all idealized and unlikely to exactly resemble the melt rate
 206 at any particular glacier, but a combination of all three can approximate many scenarios
 207 of submarine melting. However, because our goal is to examine how changes in the shape
 208 of the profile and average melt rate \bar{m} alter the stress field within the glacier, simple melt
 209 profiles serve the purpose better than more detailed submarine melt parameterizations.

210 Typical submarine melt rates around Greenland are seasonal, but have values rang-
 211 ing from 0.1 m/day to 10 m/day [*Truffer and Motyka*, 2016]. We examine rates between
 212 0.05 m/day and 5 m/day. Submarine melt is applied normal to the calving front.

Table 1. Physical parameters used in experiments

Parameter	Value
Initial ice thickness H	800 m
Initial length to thickness ratio L/H	6
Water depth D	700 m
Gravitational acceleration g	$9.8 \text{ m}\cdot\text{s}^{-2}$
Depth-averaged melt rate \bar{m}	$0.05\text{--}5.0 \text{ m}\cdot\text{day}^{-1}$
Glacier temperature T	$-20 \text{ }^\circ\text{C}$
Temperature-dependent creep parameter B	$4.088 \times 10^6 \text{ Pa}\cdot\text{day}^{1/3}$
Density of ice ρ_i	$910 \text{ kg}\cdot\text{m}^{-3}$
Density of sea water ρ_w	$1020 \text{ kg}\cdot\text{m}^{-3}$
Friction coefficient μ	$2.0 \times 10^5 \text{ Pa}\cdot\text{m}^{-1}\cdot\text{day}$

2.4 Model numerics and initial conditions

We use the open source FEniCS package [Logg *et al.*, 2012; Alnæs *et al.*, 2015] to solve the stress equilibrium equations combined with appropriate boundary conditions and the rheology of ice (Section 2.1). Each glacier was initialized as an isothermal rectangular slab on a flat bed with prescribed thickness and water depth. The initial thickness of the glacier is set to 800 m, as a representative size of major marine terminating glaciers in Greenland and Alaska (e.g. Jakobshavn, Helheim Glacier). Based on our failure criterion, only a range of ice thickness/water depth combinations are permissible at the calving front or the glacier will develop through penetrating fractures immediately, resulting in disintegration [Ma *et al.*, 2017]. This envelope of ice thickness/water depth combinations also agrees with observations around Greenland [Bassis and Walker, 2012; Ma *et al.*, 2017]. The range of water depth allowed by the stable envelope is about 90% of the ice thickness (buoyancy level) to 10 – 100 m below it. Here, the choice of water depths (700 m) is a bit below the buoyancy level (714 m) and the modeled glacier falls well within the stable envelope. Because our interest lies in the near terminus region, we set the initial length in each simulation to 6 times the thickness to avoid edge effects associated with the upstream boundary condition; we experimented with different aspect ratios and found that the stress field near the calving front was insensitive to the length above this threshold. We use a

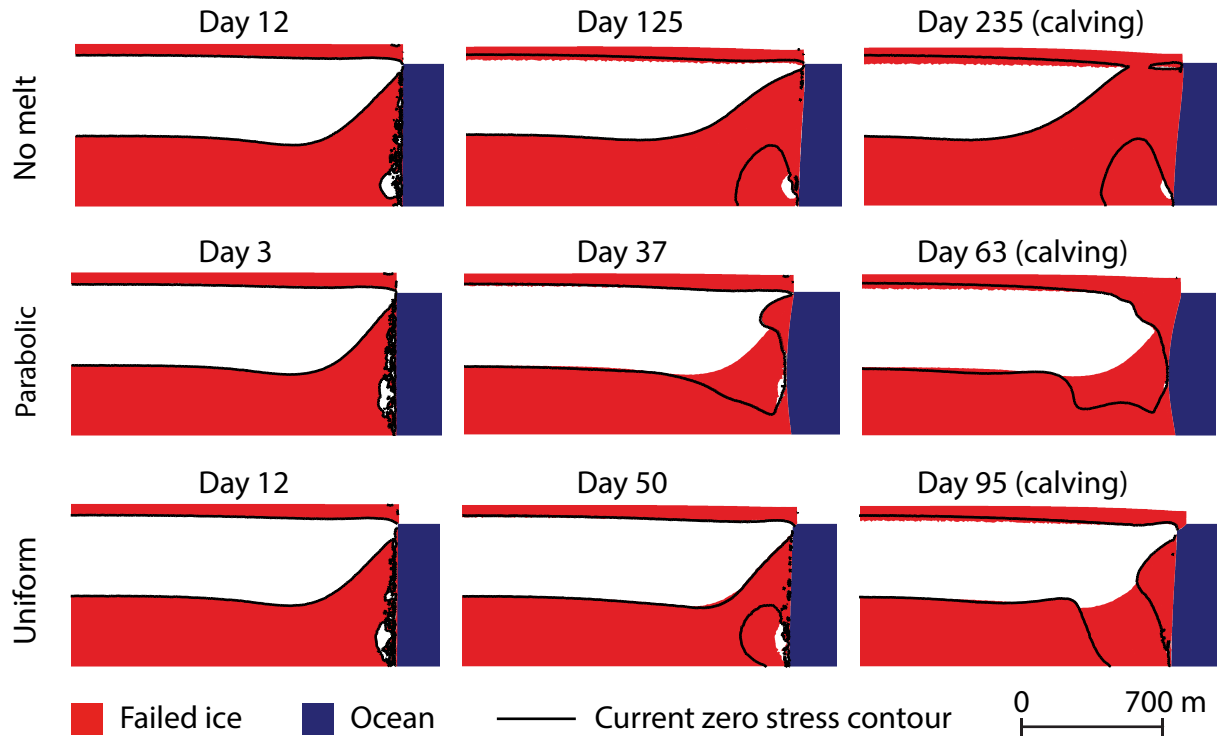
232 mesh of triangular elements and a resolution of 2% of the initial glacier thickness uni-
233 formly in both vertical and horizontal directions. At this resolution our results are insen-
234 sitive to a factor of 2 changes in resolution. During each time step (a quarter of a day),
235 the tensile and shear stress fields are calculated from the velocity solution to determine ar-
236 eas within the glacier that satisfy the tensile or shear failure criteria (Section 2.2). Then
237 we advect all nodes using the nodal velocity vector and erode the portion of the calving
238 front submerged in water according to the imposed submarine melt profile. At the end of
239 each time step, we re-mesh according to the updated glacier outline to maintain a constant
240 mesh quality throughout the simulation. The program is stopped once a calving event has
241 been observed.

261 3 Results

262 3.1 Effect of melt profile shape on stress regime

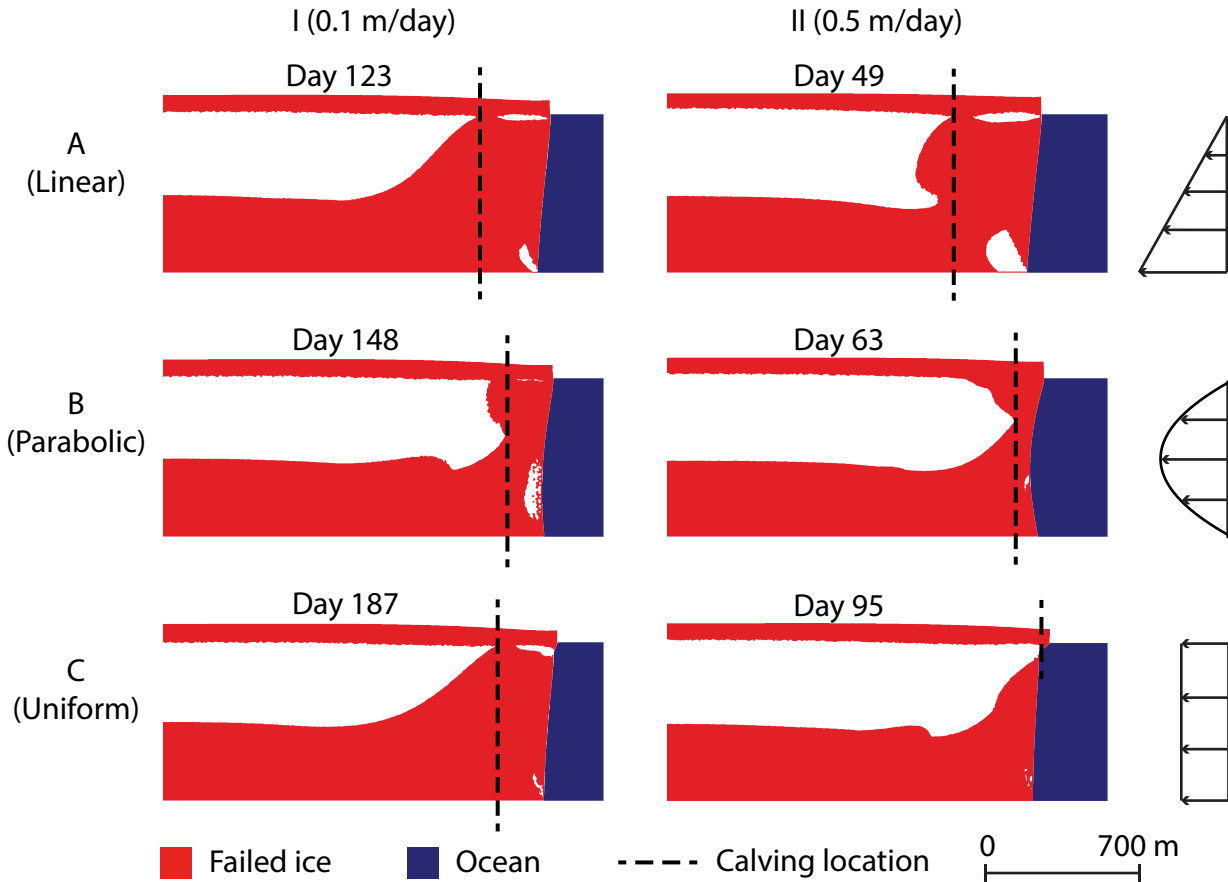
263 We first examined how changes in the shape of the glacier affect the stress field as
264 the glacier and calving front co-evolve as a function of different melt rates and profiles.
265 Fig. 2 shows three snapshots from examples: with no submarine melt, a parabolic melt
266 profile (mean melt rate 0.5 m/day) and, a uniform melt profile (melt rate 0.5 m/day) for
267 an initially 800 m thick glacier grounded in 700 m of water. Initially, failure (mostly ten-
268 sile) is concentrated in portions of the glacier above the water line as well as near the bed
269 and extends deeper into the glacier closer to the terminus (Fig. 2 left column). This is
270 a consequence of our assumption that ocean water fills all basal crevasses. For the case
271 where no melting is applied, the failure zone near the bed slowly expands and connects to
272 the surface as the glacier thins to near buoyancy (Fig. 2 top middle and top right panels).
273 When submarine melting is introduced, stress patterns become more complex and depend
274 more sensitively on the shape of the profile.

275 The pattern of stress also depends on the amplitude of submarine melt. This is il-
276 lustrated in Figure 3, which shows the stress regime at the point of calving for two differ-
277 ent mean submarine melt rates. For the linear profile (row A in Fig. 3), increased sub-
278 marine melt results in higher tensile stresses (later high shear stress too) and leads to
279 larger regions of failure that connect between the surface and bottom of the glacier. In
280 this case, submarine melt acts to increase stress and hence to promote calving. In con-
281 trast, for the parabolic and uniform profiles (middle row in Fig. 2, rows B and C in Fig.



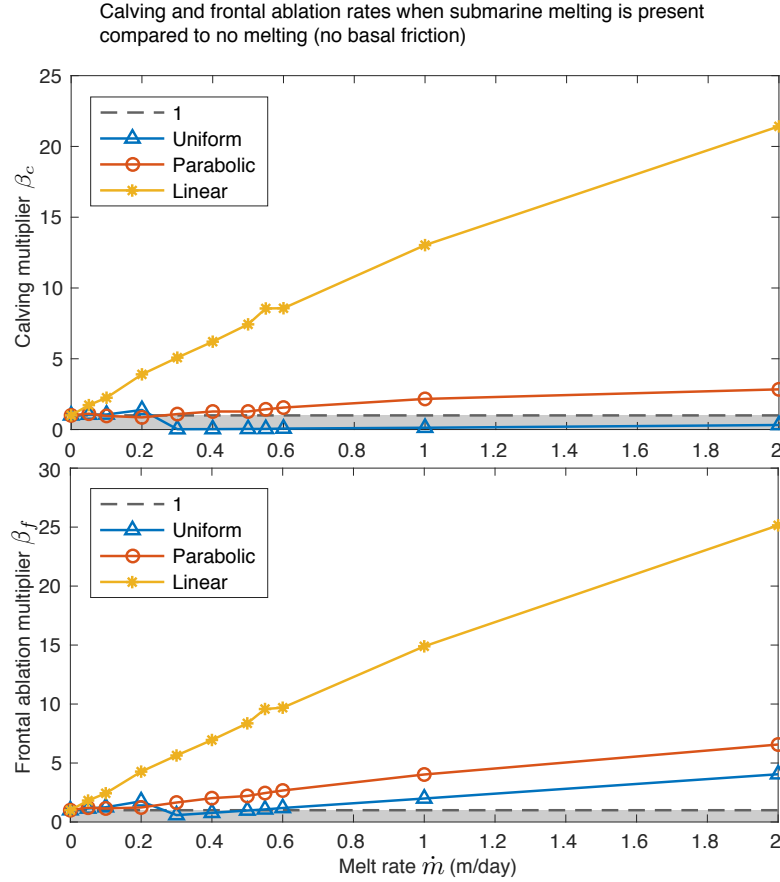
242 **Figure 2.** The evolution of stress within a tidewater glacier without basal friction. The initially 800 m thick
 243 glacier is flowing from left to right, into 700 m deep ocean (indicated by blue). These panels are cropped to
 244 show only the section of the glacier close to the calving front. Solid black lines indicate the Nye zero stress
 245 contour at the current time. The red shaded area shows accumulation of ice that has failed, reflecting the
 246 evolution and history of the glacier. White regions indicate zones of intact ice. When zones of failed ice con-
 247 nect, a calving event occurs. Top row shows three snapshots throughout the course to calving when there is
 248 no submarine melting. The middle and bottom rows show the case of a parabolic and uniform melt profile,
 249 respectively, with an average melt rate of 0.5 m/day. The first column shows the stress field at the beginning of
 250 the simulation. The second column shows the stress distribution at a point intermediate to a calving. The third
 251 column shows a situation where failed ice penetrates the entire ice thickness and a calving event occurs.

282 3), a pronounced overhang develops and the flexure associated with the overhang creates
 283 compressive stress near the bottom of the glacier, reducing the area where full thickness
 284 failure can occur and the stress regime near the calving front right beneath the developing
 285 overhang has become compressive. Compared to the linear profile, full thickness calving
 286 events simulated for the parabolic and uniform profiles are smaller in size (Fig. 3 panels
 287 IB, IIB). However, as the overhang becomes more pronounced, stresses (especially shear
 288 stress) within the overhang increase and can lead to another type of calving events: over-



252 **Figure 3.** Snap shots of zones of failed ice within a tidewater glacier at times of calving events absent of
 253 basal friction. The initially 800 m thick glacier is flowing from left to right, into 700 m deep ocean (indicated
 254 by blue). These panels are cropped to show only the section of the glacier close to the calving front. Red
 255 indicates failed ice and white is intact ice. Dashed black lines indicate locations of iceberg detachment when
 256 failed ice penetrates the entire ice thickness. Rows A, B, C show calving events under a linear, parabolic, and
 257 uniform melt profile respectively (sketched in the rightmost panels). Column I and II each corresponds to a
 258 different depth averaged melt rate: 0.1 and 0.5 m/day respectively. Panels IA, IIA, and IC show examples of a
 259 full thickness calving event. Panels IB and IIB show examples of a smaller full thickness calving event. Panel
 260 IIC shows an example of an overhang break-off.

289 hang collapse. This is especially true for the uniform melt profile when the melt rate is
 290 relatively high (Fig. 3 IIC). The same compressive stress regime can be seen from the
 291 zero stress contours (Fig. 2 bottom row last panel). In summary, we see two modes of
 292 calving: full thickness calving and overhang collapse. The type of calving event is deter-
 293 mined by both the magnitude and shape of the melt profile.

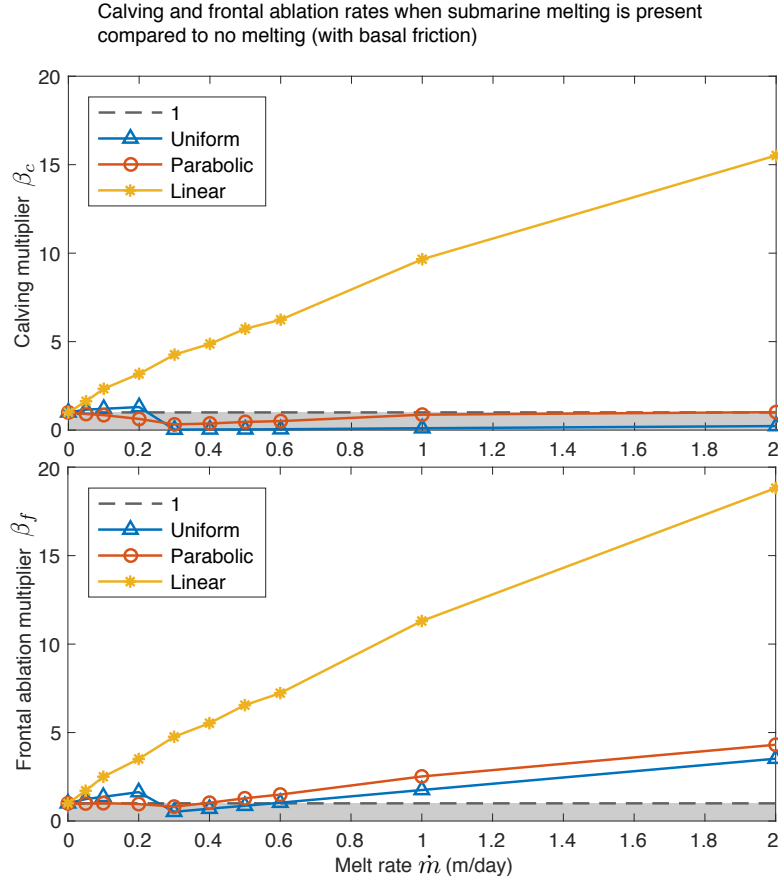


294 **Figure 4.** The effect of submarine melt on calving and frontal ablation when there is no basal friction.
 295 The top panel shows the influence of submarine melt on the calving rate multiplier while the bottom panel
 296 shows the frontal ablation rate multiplier. Yellow (stars), red (circles), and blue (triangles) lines correspond to
 297 linear, parabolic, and uniform melt profiles. The dashed line in both panels indicates a value of 1. It separates
 298 enhancement (values above the line) from suppression (values beneath the line in the shaded area).

304 3.2 Effect of submarine melting on calving and frontal ablation

305 We next sought to quantify the effect of submarine melting on the rate at which ice
 306 is lost due to calving along with the total mass lost due to frontal ablation. To do this we
 307 crudely define the ‘calving rate’ c as the area Q_c of ice breaking off divided by the time t
 308 it takes in our simulation for the ice to reach a state where failure can result in the detach-
 309 ment of an iceberg:

$$c = \frac{Q_c}{t} \quad (12)$$



299 **Figure 5.** The effect of submarine melt on calving and frontal ablation when there is basal friction. The
 300 top panel shows the influence of submarine melt on the calving rate multiplier while the bottom panel shows
 301 the frontal ablation rate multiplier. Yellow (stars), red (circles), and blue (triangles) lines correspond to linear,
 302 parabolic, and uniform melt profiles. The dashed line in both panels indicates a value of 1 separating
 303 enhancement (values above the line) from suppression (values beneath the line in the shaded area).

310 This leads to the definition of ‘frontal ablation rate’ or ‘total mass loss rate’ a to be the
 311 sum of calving rate and the product of melt rate \dot{m} and water depth D :

$$a = c + \dot{m}D \quad (13)$$

312 We use the term ‘calving rate’ and ‘frontal ablation rate’ loosely to quantify the temporal
 313 change in the stress regime associated with the emergence of through-penetrating fractures
 314 with and without submarine melting. Long term calving rates depend on upstream boundary
 315 condition and climate forcing, processes that are not accounted for in our idealized
 316 model.

Because our interest is in the role that submarine melt plays in enhancing or reducing the time it takes to develop through-penetrating fractures, we define a ‘calving rate multiplier’ β_c as the ratio of calving rate with submarine melting c_m to that without submarine melting c_0 :

$$\beta_c = \frac{c_m}{c_0}. \quad (14)$$

Similarly, we define a frontal ablation multiplier β_f as the ratio of total mass loss rate with submarine melting a_m to that without submarine melting a_0 :

$$\beta_f = \frac{a_m}{a_0} = \frac{c_m + \dot{m}D}{c_0} = \beta_c + \frac{\dot{m}D}{c_0}. \quad (15)$$

Here, a calving rate multiplier or frontal ablation multiplier greater than one ($\beta_c > 1$ or $\beta_f > 1$) indicates enhanced calving or frontal ablation relative to the submarine melt free case. In contrast, values less than one indicate suppressed calving or frontal ablation relative to the submarine melt free case.

Fig. 4 shows the calving rate and frontal ablation rate multiplier as a function of submarine melt rates ranging from 0 (no melting) to 2 m/day when there is no basal friction. The data points for the 5 m/day melt rate are not included in the figure, but the trend holds. We see three distinct responses in the simulations when the three melt profiles are applied. Applying a linear melt profile results in an almost linear increase in both calving and frontal ablation enhancement with increasing melt rates. In contrast, applying a uniform melt profile results in an initially nearly linear increase for low melt rates followed by a sharp drop-off above a threshold melt rate and then a linear increase again as melt rates further increase. Finally, applying a parabolic melt profile results in a slight decrease for low melt rates followed by a linear increase above a threshold melt rate. The specific value of the multiplier, however, depends on the shape of profile with the linear melt profile resulting in as much as a twenty-fold increase in calving rate and frontal ablation rate. This should be contrasted with the uniform and parabolic profiles, which result in more modest maximum enhancements of $\sim 200\%$ and 10% , respectively. For the parabolic profile, below ~ 0.3 m/day, the smaller berg sizes result in a small drop in calving rate multiplier. In this regime, submarine melting suppresses mass lost due to calving. We see an opposite trend for the uniform melt rate at the same melt rate. In this case, a prominent overhang develops. Bending associated with the unsupported overhang increases the compressive stress in the portion of the glacier below the overhang and high tensile and shear stress are concentrated in the overhang, resulting in the overhang break-off from the main

347 body of ice instead of a full thickness calving event. The uniform and parabolic melt pro-
348 files suppress calving for certain melt rates, but with added mass loss through submarine
349 melting we see a frontal ablation rate comparable to or higher than that without submarine
350 melting (ratio about equal to or greater than 1), except for a narrow range of melt rates for
351 the uniform melt profile.

352 **3.3 Effect of basal friction**

353 Our free-slip experiments represent significant idealizations. To examine the effect
354 of basal friction on our results, we also performed a set of simulations with a Newtonian
355 sliding law. We set the coefficient of friction such that the magnitude of basal friction is
356 between 50 and 100 kPa. The stress field when a calving event occurs in this case is very
357 similar to that without basal friction for almost all cases, except for the parabolic melt
358 profile. The difference in the stress field at the time of calving between the friction case
359 and the friction-free case is that the former shows larger compressive stress at the bottom
360 of the glacier near the calving front, while the latter shows tensile stress. The inclusion
361 of friction decreases the velocity of ice at the ice-bed interface and this results in larger
362 compressive stresses. Consequently, comparing Fig. 5 with Fig. 4, we see that the calv-
363 ing behavior corresponding to each melt profile remains qualitatively similar regardless
364 of basal friction and the monotonic increase for the linear melt profile, the slow increase
365 after decrease for the parabolic melt profile, as well as the decrease after the initial in-
366 crease for the uniform profile are still present. However, the magnitude of the calving and
367 frontal ablation multipliers are slightly smaller and the transition melt rate between en-
368 hancement and suppression of calving for the parabolic and uniform melt profiles shifts to
369 ~ 0.2 m/day. Moreover, the calving multiplier for the parabolic profile when basal fric-
370 tion is present is lower compared to the case with no friction for melt rates up to 2 m/day.
371 The resistance at the bed creates a more compressive stress regime near the bottom part of
372 the glacier, making it more difficult for failure zones to extend and connect throughout the
373 entire ice thickness. We anticipate that more complex basal sliding laws would affect our
374 quantitative results, but that we would see similar qualitative trends so long as the glacier
375 remains in the rapidly sliding regime.

3.4 Multiple calving events

Our idealized simulations all started with rectangular geometries and thus the first calving event in our model may not be representative of the true calving rate. To examine the effect of multiple calving events, we performed a final simulation in which we simulated a second calving event after the initial break-off event. To do this, we simulated calving events by instantaneously removing all ice seaward of the location where we simulate through-penetrating fractures. In the absence of submarine melt, our simulated glacier evolves until it reaches buoyancy without experiencing another calving event. In contrast, when submarine melt is applied to the calving front, the shape of the calving front continues to evolve and we do observe a second calving event before the glacier reaches buoyancy. For modest melt rates between 0.1 and 0.5 m/day this second calving event takes longer than the first calving event, but faster than in the absence of submarine melt (where we do not observe a second calving event prior to the formation of a floating ice tongue). In these cases, submarine melt appears to enhance total front ablation. However, these simulations do not account for buoyancy induced calving, which could result in through penetration fractures upstream of the calving front when the glacier approaches flotation. This suggests that, qualitatively at least, submarine melt may enhance total frontal ablation for multiple calving events. However, our estimated long term calving fluxes are less certain because the longer time scale evolution of the glacier associated with multiple calving events depends on a group of factors that we have not considered. For example, the effect of surface mass balance and variations in bed geometry are likely to become more important in controlling the timing of calving events when the modeled time period extends well beyond 1 year. Instead, our simulations show that submarine melt alters the geometry of the calving front and this change in geometry has a first-order effect on the stress regime near the calving front and this change is likely to translate into a change in the calving rate of glaciers.

4 Discussion

Our simulations show that submarine melting, by changing the morphology of the calving front, exerts a first-order control on the near terminus stress regime state of marine terminating glaciers. This effect can, in some cases, increase or suppress calving. The magnitude—and even the sign of the interaction between submarine melting and calving—depends on both the amount of submarine melt and the vertical distribution of melt over

408 the calving front. The shape of the melt profile plays such an important role in determin-
409 ing the interplay between calving and submarine melting because of the effects different
410 melt profiles have on the shape of the calving face. Undercutting at the calving front re-
411 sults in unsupported mass; the size and shape of this mass can result in stabilizing com-
412 pressive stresses upstream from the overhang or destabilizing tensile stresses close to the
413 calving front. The uniform melt profile case is most effective in suppressing calving; the
414 linear melt profile tends to enhance calving. Ultimately, however, the overhang grows large
415 enough that it becomes unstable and detaches.

416 Our simulations identify different types of calving in response to submarine melt-
417 ing. When submarine melting is present, the erosion of ice from the calving front allows
418 glacier ice to flow into the calving front and partially compensate for the change in the
419 shape of the calving front. Consequently, the glacier thins faster and reaches a full thick-
420 ness calving event earlier in our simulations than in the absence of submarine melt. Be-
421 cause more glacier ice is being removed from the calving front halfway underwater than at
422 the waterline or the bottom, the parabolic melt profile renders the extra mass near the sur-
423 face unsupported so that the stress field becomes more compressive, resulting in a slightly
424 reduced calving event size. As the melt rate further increases, the time to calving reduces.
425 Although the calving size shows little change, calving rate increases with melt rate. For
426 the uniform melt profile case, when enough mass is removed from the calving front below
427 the waterline, a large overhang develops. Similar to the parabolic case, the unsupported
428 overhang has a compressive effect on the part of ice underneath it and is less favorable for
429 the growth of tensile failure. Nonetheless, the portion where the overhang connects to the
430 main body of ice becomes more prone to failure due to a concentrated area of high shear
431 and high tensile stress around the entire overhang. The more rapidly ice is melted away,
432 the earlier the overhang becomes large enough to detach. The linear submarine melt pro-
433 file case is different from the other two cases because removing more ice from the bottom
434 and creating a sloping calving front promotes full thickness calving by increasing the calv-
435 ing size significantly. The faster ice is being removed from the bottom, the more unstable
436 the calving front becomes and the easier it is for a full thickness calving event to occur.

437 Our results are relatively consistent with observations. For example, *Bartholomaeus*
438 *et al.* [2013] found that, at least during the summer when ocean temperatures were large
439 ($> 10^{\circ}\text{C}$), the mass lost from Yahtse Glacier, Alaska due to submarine melting accounted
440 for nearly all of the submarine mass loss. This corresponds to our simulations where sub-

441 marine melt rates are large compared to the ice flow velocity—especially if submarine
442 melt rates are approximately uniform along the calving front. Our model would predict
443 this regime is controlled by overhang collapse, although narrow full thickness bergs could
444 also occasionally detach. Similarly, our model is consistent with the relatively warm ocean
445 temperatures controlling frontal ablation of Svalbard glaciers [Luckman *et al.*, 2015] be-
446 cause frontal ablation is controlled by submarine melting for large melt rates.

447 The most intriguing result from our simulations is that submarine melt can both in-
448 crease and reduce calving, depending on the shape of the melt profile. An initial increase
449 in melt rate can increase calving for the uniform profile. However, as the melt rate con-
450 tinues to increase, we see a transition to smaller icebergs and this reduced iceberg size
451 decreases the mass lost due to calving. On the other hand, slightly reduced calving has
452 been shown from the model results for small melt rates using the parabolic melt profile
453 because of the slightly reduced size of icebergs. Eventually, as the submarine melt contin-
454 ues to increase, calving flux increases again; this is a consequence of the fact that smaller
455 bergs detach more frequently. Both the uniform and parabolic melt profiles can moderately
456 increase calving. In contrast, for the linear profile, we see increased calving for all melt
457 rates and more than an order of magnitude increase for higher melt rates. This may partly
458 explain the increased calving many tidewater glaciers experience during the summer [e.g.,
459 *Amundson et al.*, 2008, 2010], although our model neglects water in surface crevasses and
460 the presence of *mélange* that has been speculated to buttress the calving front. Despite
461 the fact that submarine melting can suppress calving, the rate of total frontal ablation gen-
462 erally increases with increasing melt rate—with the exception of a narrow range of melt
463 rates. Submarine melt, however, does alter the total frontal ablation along with the parti-
464 tioning between calving and melting.

465 **5 Conclusion**

466 Our simulations show that vertical distribution of submarine melt along the calv-
467 ing front results in markedly different glaciological stress regimes. A consequence of this
468 is that submarine melting can increase calving by more than an order of magnitude or
469 suppress calving (nearly) entirely, according to our estimate of calving rate based on the
470 first calving event. The distinction between these two effects is controlled by the relative
471 strength of depth averaged melt rate and, more significantly, the vertical distribution of
472 submarine melt. Although we imposed idealized melt profiles in our simulations, future

473 simulations could more accurately model the interplay between calving and submarine
474 melting either using full ocean circulation models or simpler plume models coupled with
475 an ice sheet model.

476 Our results also suggest that attempts to understand the interplay between calving
477 and submarine melting need to consider factors that affect the local melt profile and its
478 magnitude along with the effect these have on the glaciological stress regime response.
479 Because of the dependence on the magnitude and vertical distribution of the submarine
480 melt profile, extrapolating observational results from a single or small set of glaciers could
481 prove to be misleading. Moreover, as *Luckman et al.* [2015] and *Rignot et al.* [2016] both
482 pointed out, the importance of submarine frontal melting depends on its relative strength
483 compared to ice dynamics at the glacier terminus. Removing ice from the calving front
484 can destabilize the glacier and cause ice to flow into the terminus area to compensate for
485 the effect of melting. However, if the mass is being eroded away too quickly, the resulting
486 instability could be hard to compensate for and a transition from full thickness bergs to
487 smaller bergs or overhang collapse could occur.

488 Our model is relatively simple and omits several important processes, including lat-
489 eral geometry and mass balance. Nonetheless, when considering the evolution of glaciers
490 in a warming climate, we may need to consider more than just the magnitude of subma-
491 rine melt; we may also need to know the precise three-dimensional shape. This in turn,
492 will require a more in-depth knowledge of the three-dimensional circulation of water in
493 fjords and perhaps more detailed coupling between ice sheet/glacier models and ocean
494 models.

495 **Acknowledgments**

496 We would like to thank the editors and both reviewers. This work was supported by Na-
497 tional Science Foundation grant ANT 114085, National Oceanic and Atmospheric Admin-
498 istration, Climate Process Team: Iceberg Calving grant NA13OAR4310096 and National
499 Science Foundation grant PLR-131568. All numerical information is provided in the ta-
500 bles and figures, and was produced by solving the equations stated in the paper. Codes
501 used to generate the results can be found on GitHub at <https://goo.gl/R4DwVZ>

502 **References**503 **References**

- 504 Alnæs, M. S., J. Blechta, J. Hake, A. Johansson, B. Kehlet, A. Logg, C. Richardson,
505 J. Ring, M. E. Rognes, and G. N. Wells (2015), The FEniCS Project Version 1.5,
506 *Archive of Numerical Software*, 3(100), doi:10.11588/ans.2015.100.20553.
- 507 Amundson, J., M. Truffer, M. Lüthi, M. Fahnestock, M. West, and R. Motyka (2008),
508 Glacier, fjord, and seismic response to recent large calving events, Jakobshavn Isbræ,
509 Greenland, *Geophysical Research Letters*, 35(22), L22501.
- 510 Amundson, J. M., M. Fahnestock, M. Truffer, J. Brown, M. P. Lüthi, and R. J. Motyka
511 (2010), Ice mélange dynamics and implications for terminus stability, Jakobshavn Isbræ,
512 Greenland, *Journal of Geophysical Research: Earth Surface*, 115(F1), F01005.
- 513 Bartholomäus, T. C., C. F. Larsen, and S. O’Neel (2013), Does calving matter? Evidence
514 for significant submarine melt, *Earth and Planetary Science Letters*, 380, 21–30.
- 515 Bassis, J. N., and C. C. Walker (2012), Upper and lower limits on the stability of calving
516 glaciers from the yield strength envelope of ice, *Proceedings of the Royal Society of Lon-*
517 *don A: Mathematical, Physical and Engineering Sciences*, 468(2140), 913–931.
- 518 Benn, D. I., C. R. Warren, and R. H. Mottram (2007), Calving processes and the dynam-
519 ics of calving glaciers, *Earth-Science Reviews*, 82(3), 143–179.
- 520 Benn, D. I., J. Åström, T. Zwinger, J. Todd, F. M. Nick, S. Cook, N. R. J. Hulton, and
521 A. Luckman (2017), Melt-under-cutting and buoyancy-driven calving from tidewater
522 glaciers: new insights from discrete element and continuum model simulations, *Journal*
523 *of Glaciology*, 63(240), 691–702.
- 524 Colgan, W., H. Rajaram, W. Abdalati, C. McCutchan, R. Mottram, M. S. Moussavi, and
525 S. Grigsby (2016), Glacier crevasses: Observations, models, and mass balance implica-
526 tions, *Reviews of Geophysics*, 54(1), 119–161.
- 527 Cook, S., I. Rutt, T. Murray, A. Luckman, T. Zwinger, N. Selmes, A. Goldsack, and
528 T. James (2014), Modelling environmental influences on calving at Helheim Glacier
529 in eastern Greenland, *The Cryosphere*, 8(3), 827–841.
- 530 Enderlin, E. M., and I. M. Howat (2013), Submarine melt rate estimates for floating ter-
531 mini of Greenland outlet glaciers (2000–2010), *Journal of Glaciology*, 59(213), 67–75.
- 532 Enderlin, E. M., I. M. Howat, S. Jeong, M.-J. Noh, J. H. Angelen, and M. R. Broeke
533 (2014), An improved mass budget for the Greenland ice sheet, *Geophysical Research*
534 *Letters*, 41(3), 866–872.

- 535 Frederking, R. M. W., O. J. Svec, and G. W. Timco (1988), On measuring the shear
536 strength of ice, *Tech. rep.*, National Research Council Canada, Institute for Research in
537 Construction.
- 538 Glen, J. W. (1955), The creep of polycrystalline ice, *Proceedings of the Royal Society of*
539 *London A: Mathematical, Physical and Engineering Sciences*, 228(1175), 519–538.
- 540 Harper, J. T., N. Humphrey, and W. T. Pfeffer (1998), Crevasse patterns and the strain-rate
541 tensor: a high-resolution comparison, *Journal of Glaciology*, 44(146), 68–76.
- 542 Joughin, I., W. Abdalati, and M. Fahnestock (2004), Large fluctuations in speed on Green-
543 land’s Jakobshavn Isbræ glacier, *Nature*, 432(7017), 608–610.
- 544 Joughin, I., I. M. Howat, M. Fahnestock, B. Smith, W. Krabill, R. B. Alley, H. Stern,
545 and M. Truffer (2008), Continued evolution of Jakobshavn Isbræ following its rapid
546 speedup, *Journal of Geophysical Research: Earth Surface*, 113(F4), F04006.
- 547 Krug, J., G. Durand, O. Gagliardini, and J. Weiss (2015), Modelling the impact of sub-
548 marine frontal melting and ice mélange on glacier dynamics, *The Cryosphere*, 9, 989–
549 1003.
- 550 Logg, A., K.-A. Mardal, G. N. Wells, et al. (2012), *Automated Solution of Differential*
551 *Equations by the Finite Element Method*, Springer, doi:10.1007/978-3-642-23099-8.
- 552 Luckman, A., D. I. Benn, F. Cottier, S. Bevan, F. Nilsen, and M. Inall (2015), Calving
553 rates at tidewater glaciers vary strongly with ocean temperature, *Nature Communica-*
554 *tions*, 6, 8566–8572.
- 555 Ma, Y., C. S. Tripathy, and J. N. Bassis (2017), Bounds on the calving cliff height of ma-
556 rine terminating glaciers, *Geophysical Research Letters*, 44(3), 1369–1375.
- 557 Moon, T., I. Joughin, B. Smith, and I. Howat (2012), 21st-century evolution of Greenland
558 outlet glacier velocities, *Science*, 336(6081), 576–578.
- 559 Moon, T., I. Joughin, B. Smith, M. R. Broeke, W. J. Berg, B. Noël, and M. Usher (2014),
560 Distinct patterns of seasonal Greenland glacier velocity, *Geophysical research letters*,
561 41(20), 7209–7216.
- 562 Morlighem, M., J. Bondzio, H. Seroussi, E. Rignot, E. Larour, A. Humbert, and S. Rebuffi
563 (2016), Modeling of Store Gletscher’s calving dynamics, West Greenland, in response to
564 ocean thermal forcing, *Geophysical Research Letters*, 43(6), 2659–2666.
- 565 Motyka, R. J., L. Hunter, K. A. Echelmeyer, and C. Connor (2003), Submarine melting at
566 the terminus of a temperate tidewater glacier, LeConte Glacier, Alaska, U.S.A., *Annals*
567 *of Glaciology*, 36(1), 57–65.

- 568 Nick, F. M., C. J. van der Veen, A. Vieli, and D. I. Benn (2010), A physically based calving
569 model applied to marine outlet glaciers and implications for the glacier dynamics,
570 *Journal of Glaciology*, 56(199), 781–794.
- 571 Nye, J. F. (1955), Comments on Dr Loewe’s letter and notes on crevasses, *Journal of*
572 *Glaciology*, 2(17), 512–514.
- 573 O’Leary, M., and P. Christoffersen (2013), Calving on tidewater glaciers amplified by sub-
574 marine frontal melting, *The Cryosphere*, 7(1), 119–128.
- 575 Petrovic, J. J. (2003), Review mechanical properties of ice and snow, *Journal of Materials*
576 *Science*, 38(1), 1–6.
- 577 Rignot, E., and P. Kanagaratnam (2006), Changes in the velocity structure of the Green-
578 land Ice Sheet, *Science*, 311(5763), 986–990.
- 579 Rignot, E., J. Box, E. Burgess, and E. Hanna (2008), Mass balance of the Greenland ice
580 sheet from 1958 to 2007, *Geophysical Research Letters*, 35(20), L20502.
- 581 Rignot, E., M. Koppes, and I. Velicogna (2010), Rapid submarine melting of the calving
582 faces of West Greenland glaciers, *Nature Geoscience*, 3(3), 187–191.
- 583 Rignot, E., I. Fenty, Y. Xu, C. Cai, and C. Kemp (2015), Undercutting of marine-
584 terminating glaciers in West Greenland, *Geophysical Research Letters*, 42(14), 5909–
585 5917.
- 586 Rignot, E., Y. Xu, D. Menemenlis, J. Mouginot, B. Scheuchl, X. Li, M. Morlighem,
587 H. Seroussi, M. van den Broeke, I. Fenty, C. Cai, L. An, and B. de Fleurian (2016),
588 Modeling of ocean-induced ice melt rates of five west Greenland glaciers over the past
589 two decades, *Geophysical Research Letters*, 43(12), 6374–6382.
- 590 Röhl, K. (2006), Thermo-erosional notch development at fresh-water-calving Tasman
591 Glacier, New Zealand, *Journal of Glaciology*, 52(177), 203–213.
- 592 Schulson, E. M. (1999), The structure and mechanical behavior of ice, *Journal of the Min-*
593 *erals, Metals & Materials Society*, 51(2), 21–27.
- 594 Sciascia, R., F. Straneo, C. Cenedese, and P. Heimbach (2013), Seasonal variability of
595 submarine melt rate and circulation in an East Greenland fjord, *Journal of Geophysical*
596 *Research: Oceans*, 118(5), 2492–2506.
- 597 Slater, D. A., P. W. Nienow, D. N. Goldberg, T. R. Cowton, and A. J. Sole (2017), A
598 model for tidewater glacier undercutting by submarine melting, *Geophysical Research*
599 *Letters*, 44(5), 2360–2368.

- 600 Todd, J., and P. Christoffersen (2014), Are seasonal calving dynamics forced by buttress-
601 ing from ice mélange or undercutting by melting? Outcomes from full-stokes simula-
602 tions of Store Gletscher, West Greenland, *The Cryosphere*, 8(6), 2353–2365.
- 603 Todd, J., P. Christoffersen, T. Zwinger, P. Råback, N. Chauché, D. Benn, A. Luckman,
604 J. Ryan, N. Toberg, D. Slater, et al. (2018), A Full-Stokes 3-D Calving Model Applied
605 to a Large Greenlandic Glacier, *Journal of Geophysical Research: Earth Surface*, 123(3),
606 410–432.
- 607 Truffer, M., and R. J. Motyka (2016), Where glaciers meet water: Subaqueous melt and
608 its relevance to glaciers in various settings, *Reviews of Geophysics*, 54(1), 220–239.
- 609 van den Broeke, M., J. Bamber, J. Ettema, E. Rignot, E. Schrama, W. J. van de Berg,
610 E. van Meijgaard, I. Velicogna, and B. Wouters (2009), Partitioning recent Greenland
611 mass loss, *Science*, 326(5955), 984–986.
- 612 van der Veen, C. J. (2002), Calving glaciers, *Progress in Physical Geography*, 26(1), 96–
613 122.
- 614 van der Veen, C. J. (2013), *Fundamentals of glacier dynamics*, CRC Press.
- 615 Xu, Y., E. Rignot, I. Fenty, D. Menemenlis, and M. Flexas (2013), Subaqueous melting of
616 Store Glacier, west Greenland from three-dimensional, high-resolution numerical model-
617 ing and ocean observations, *Geophysical Research Letters*, 40(17), 4648–4653.

Figure 1.

Author Manuscript

Free slip
in vertical
direction



Traction-free on surface

Flow direction

H

z

x

D

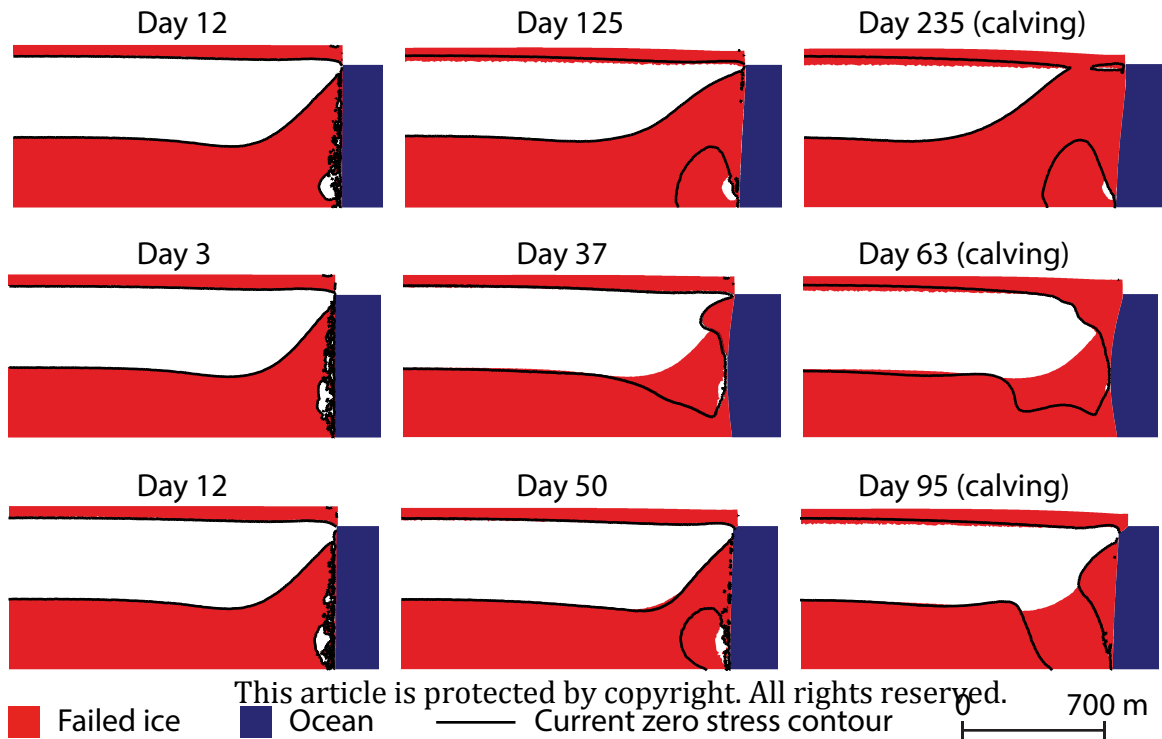
This article is protected by copyright

Free slip at bed

Melted away by water

Figure2.

Author Manuscript



This article is protected by copyright. All rights reserved.

Figure 3.

Author Manuscript

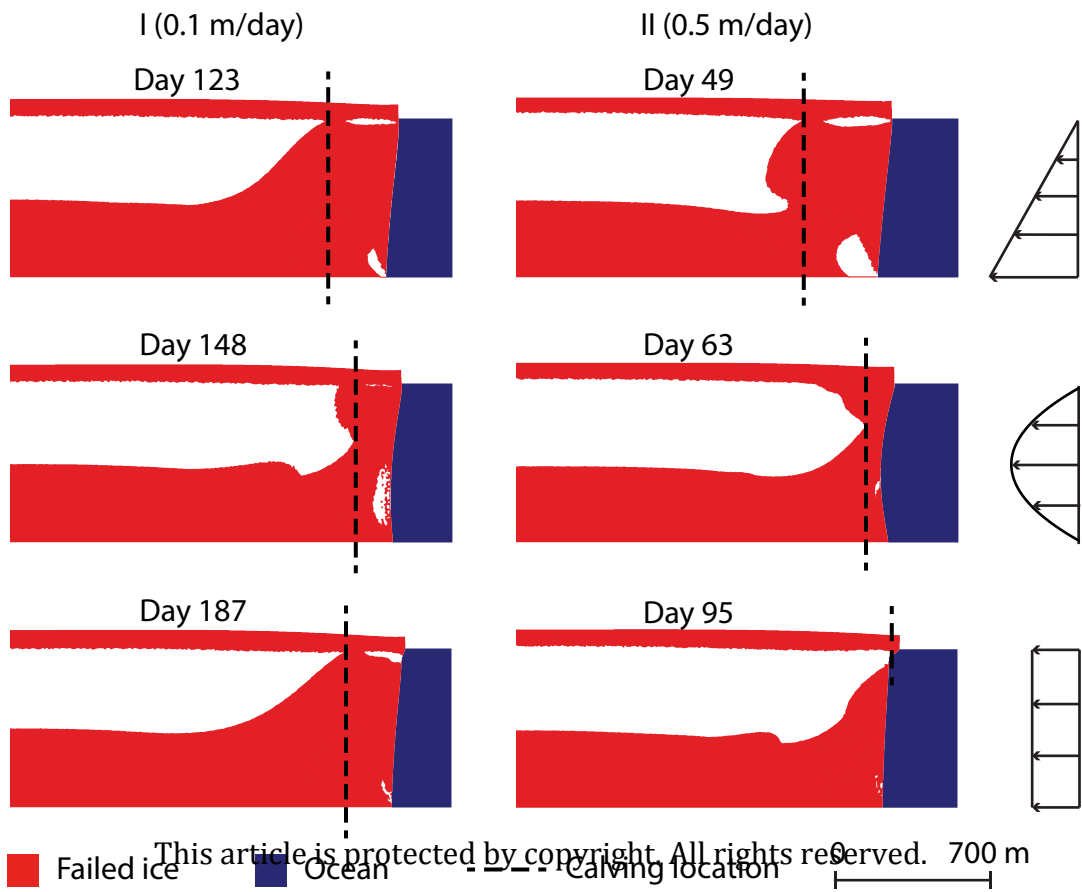


Figure 4.

Author Manuscript

Calving and frontal ablation rates when submarine melting is present compared to no melting (no basal friction)

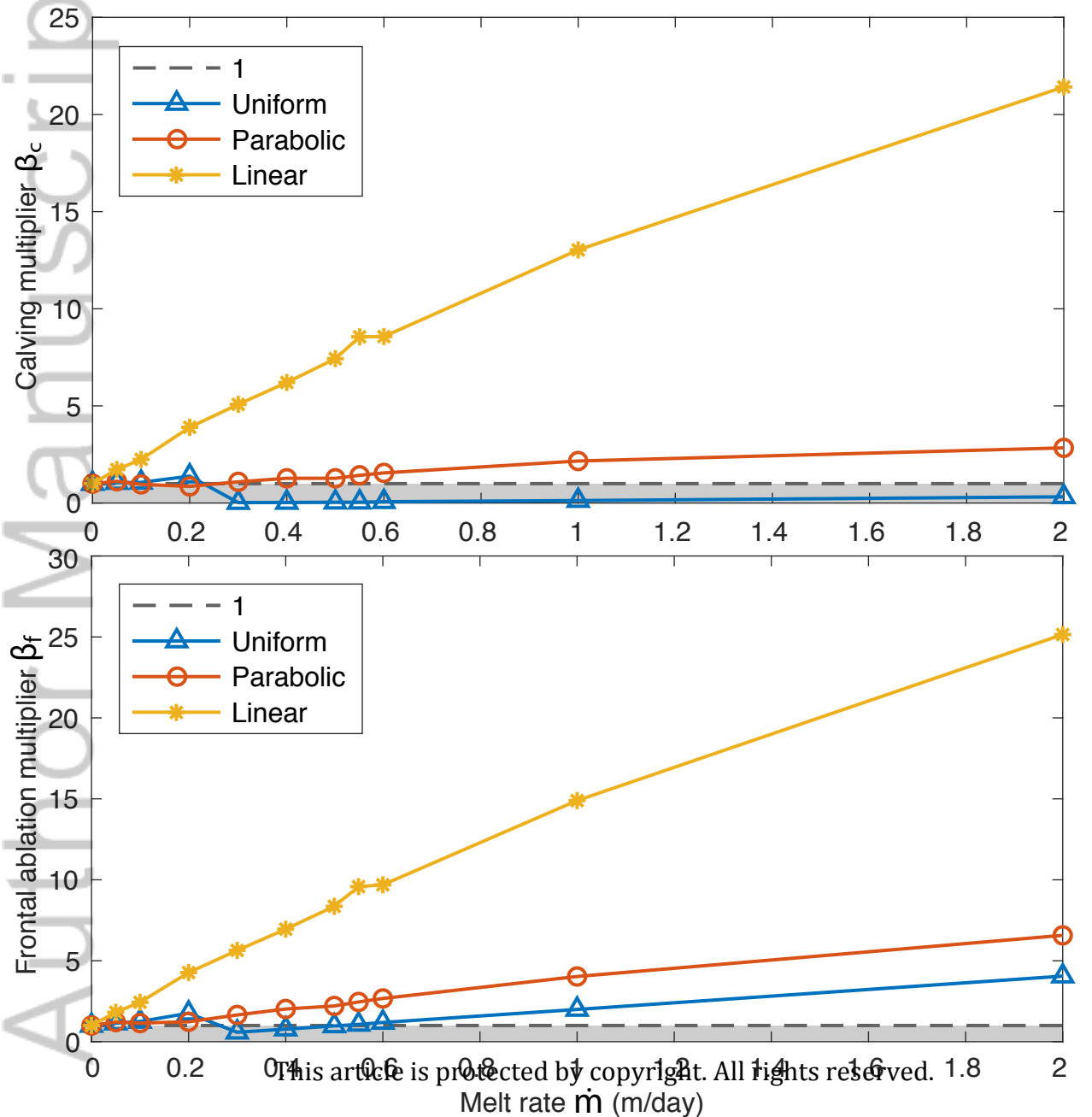
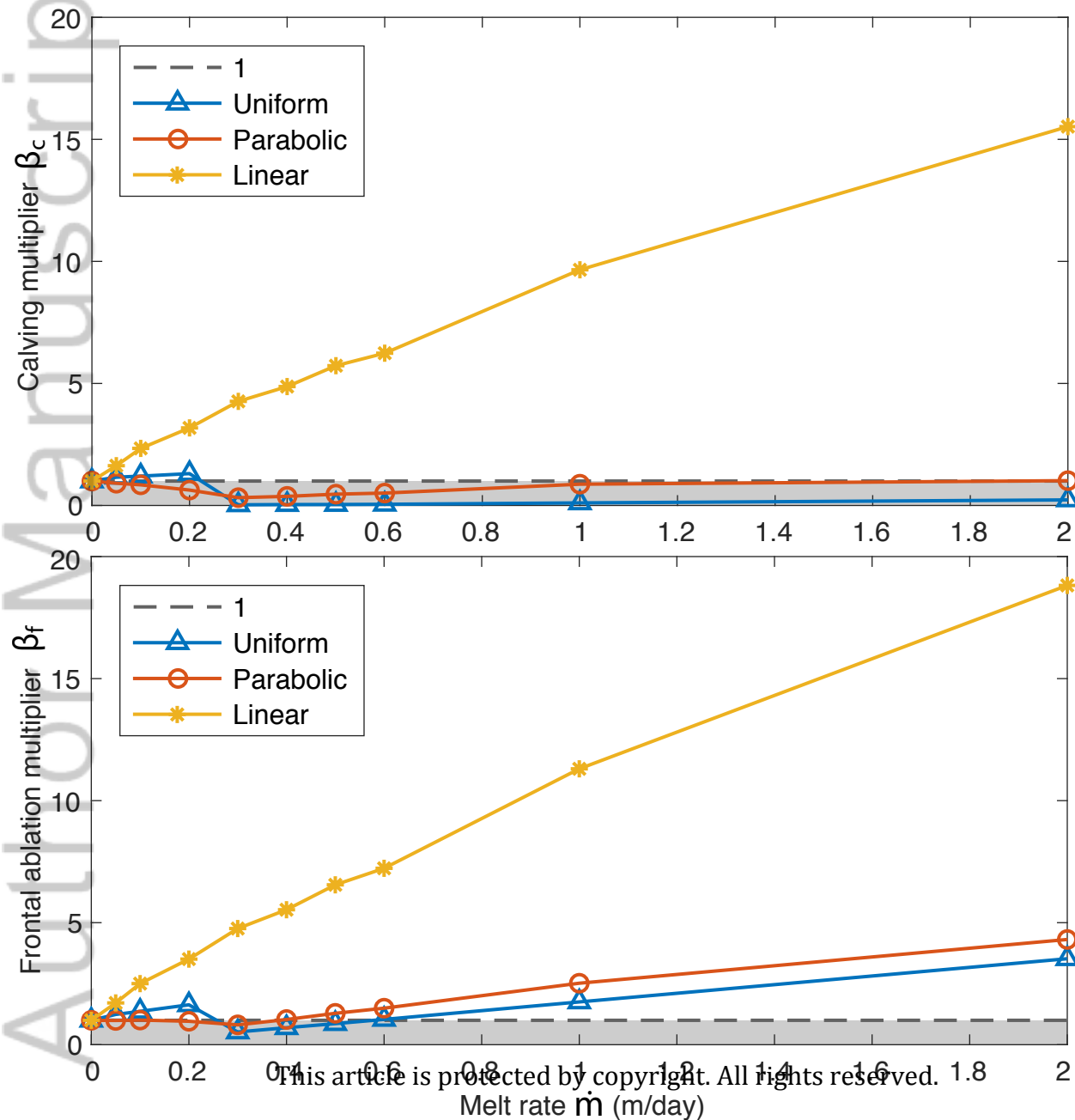


Figure 5.

Author Manuscript

Calving and frontal ablation rates when submarine melting is present compared to no melting (with basal friction)



Free slip
in vertical
direction

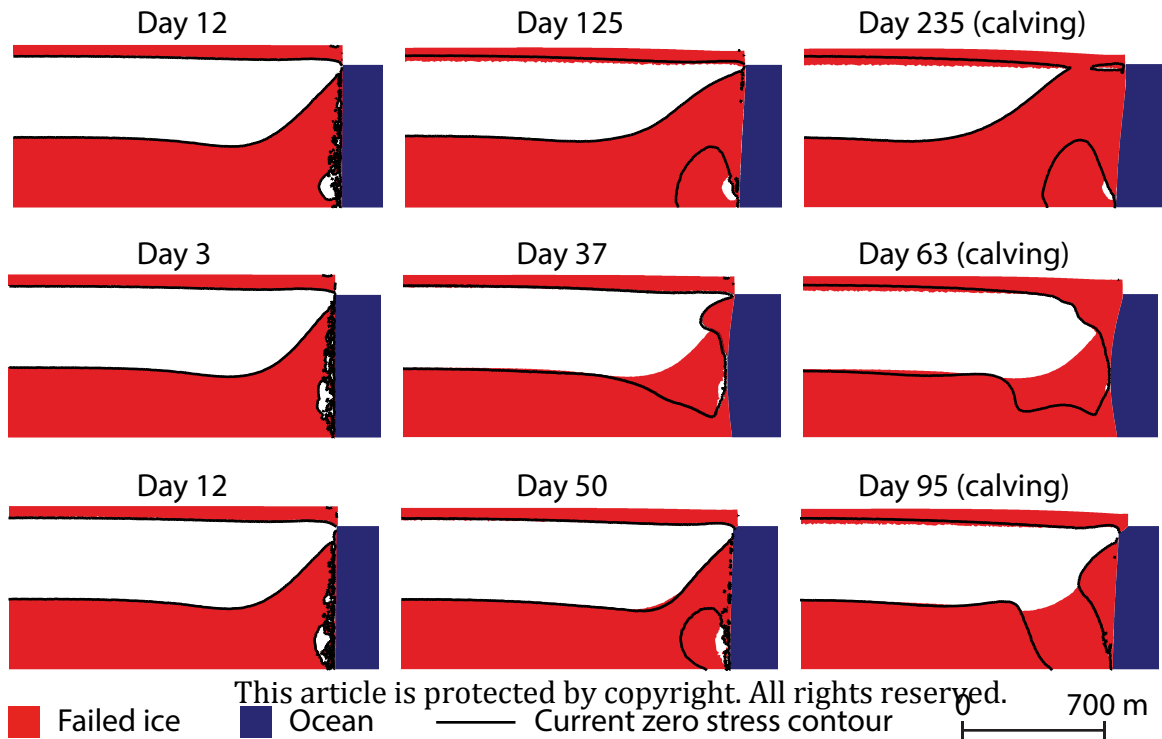
Traction-free on surface



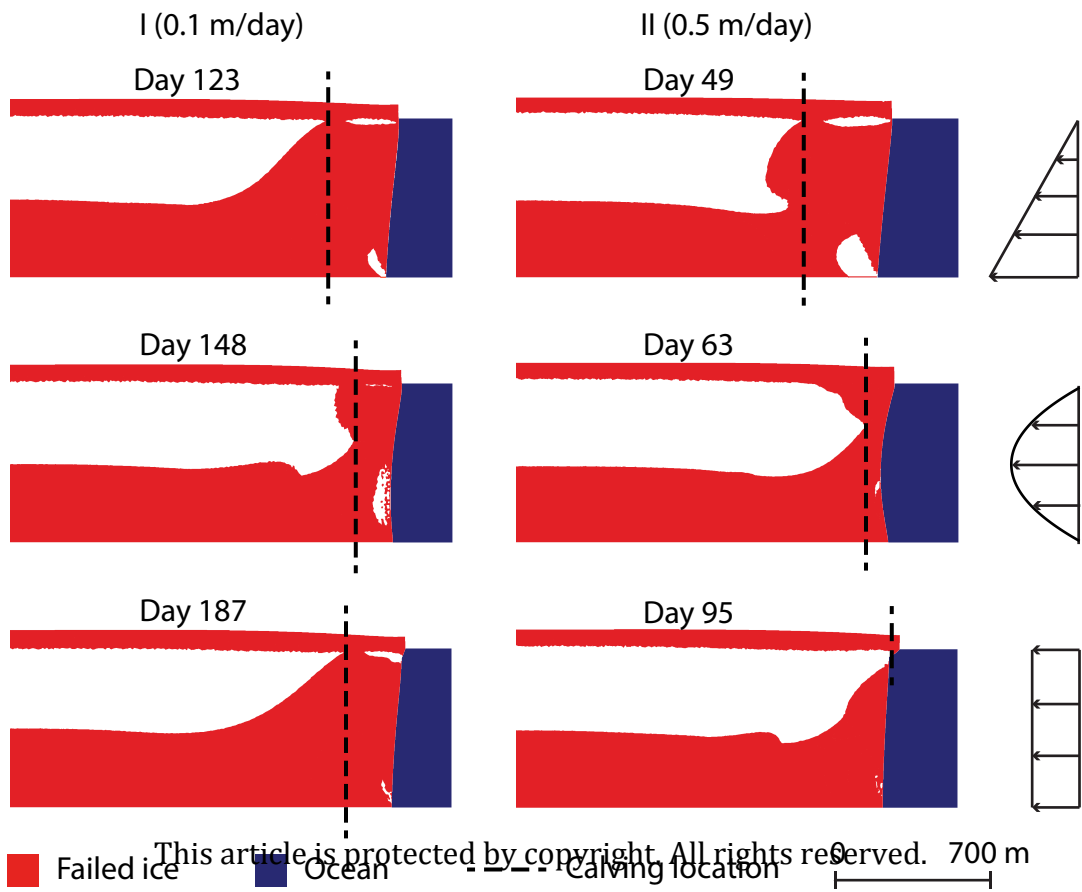
This article is protected by copyright

Free slip at bed

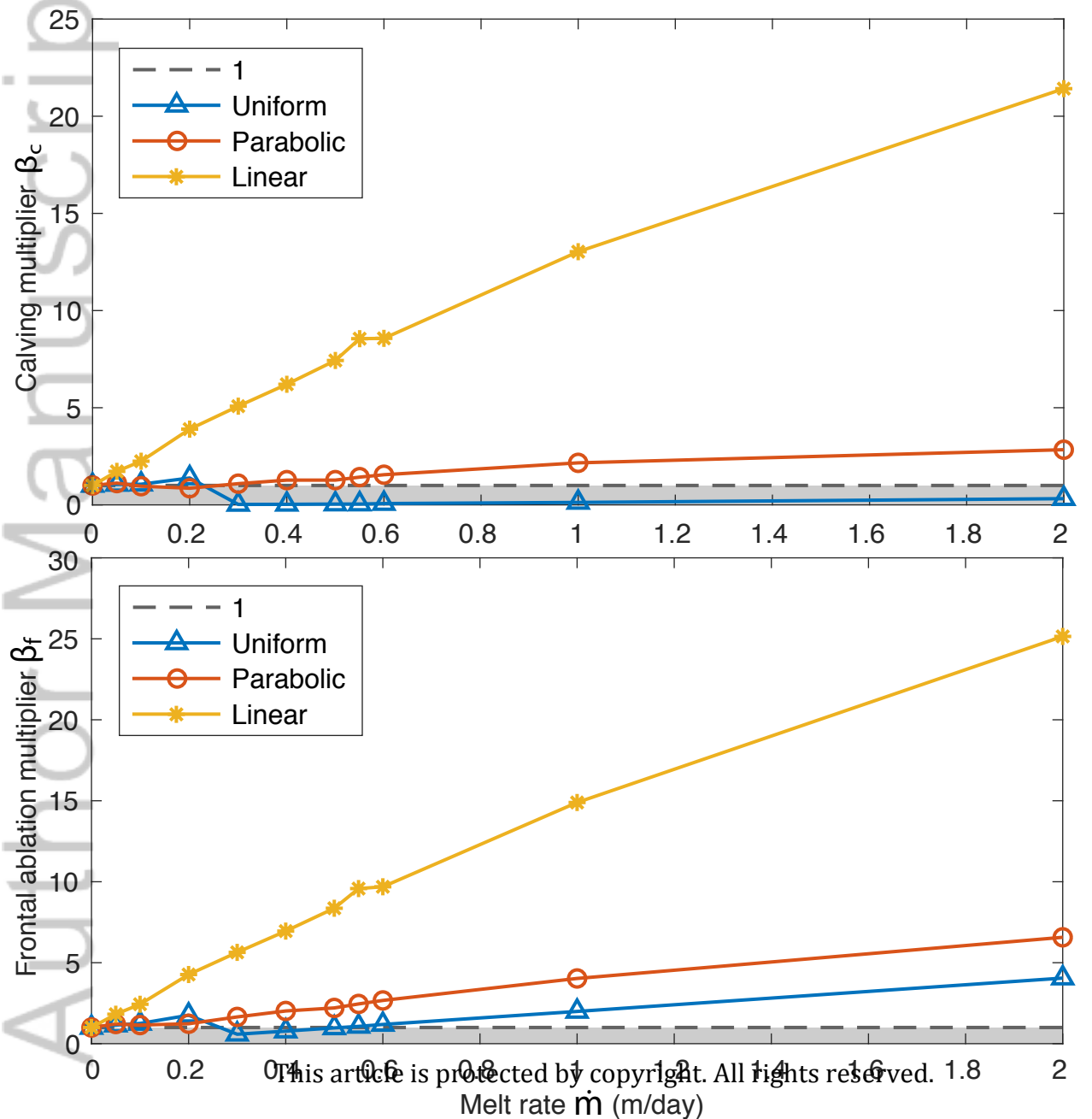
Melted away by water



This article is protected by copyright. All rights reserved.



Calving and frontal ablation rates when submarine melting is present compared to no melting (no basal friction)



Calving and frontal ablation rates when submarine melting is present compared to no melting (with basal friction)

